

Beyond Stationarity: Rethinking Codebook Collapse in Vector Quantization

Hao Lu^{1*} Onur C. Koyun¹ Yongxin Guo¹ Zhengjie Zhu¹ Abbas Alili¹ Metin Nafi Gurcan¹

¹Wake Forest University School of Medicine, Winston-Salem, NC, USA

{Hao.Lu, Onur.Koyun, Abbas.Alili}@advocatehealth.org

{Yongxin.Guo, Zhengjie.Zhu, Metin.Gurcan}@wfusm.edu

Abstract

Vector Quantization (VQ) underpins many modern generative frameworks such as VQ-VAE, VQ-GAN, and latent diffusion models. Yet, it suffers from the persistent problem of codebook collapse, where a large fraction of code vectors remains unused during training. This work provides a new theoretical explanation by identifying the non-stationary nature of encoder updates as the fundamental cause of this phenomenon. We show that as the encoder drifts, unselected code vectors fail to receive updates and gradually become inactive. To address this, we propose two new methods: Non-Stationary Vector Quantization (NS-VQ), which propagates encoder drift to non-selected codes through a kernel-based rule, and Transformer-based Vector Quantization (TransVQ), which employs a lightweight mapping to adaptively transform the entire codebook while preserving convergence to the k -means solution. Experiments on the CelebA-HQ dataset demonstrate that both methods achieve near-complete codebook utilization and superior reconstruction quality compared to baseline VQ variants, providing a principled and scalable foundation for future VQ-based generative models. The code is available at: <https://github.com/CAIR-LAB-WFUSM/NS-VQ-TransVQ.git>

Keywords: Vector Quantization, Codebook Collapse, Non-stationary Encoder, NS-VQ / TransVQ, Latent Generative Models, Codebook Utilization

1. Introduction

Vector Quantization (VQ) has long been a fundamental technique in signal processing, offering a way to represent continuous data by discrete codes [1]. Since its successful integration into Variational Autoencoders (VQ-VAE) by [2], VQ has become the backbone of many state-of-the-art generative frameworks, including VQ-GAN [3] and Latent Diffusion Models (LDM) [4]. In addition, VQ-based

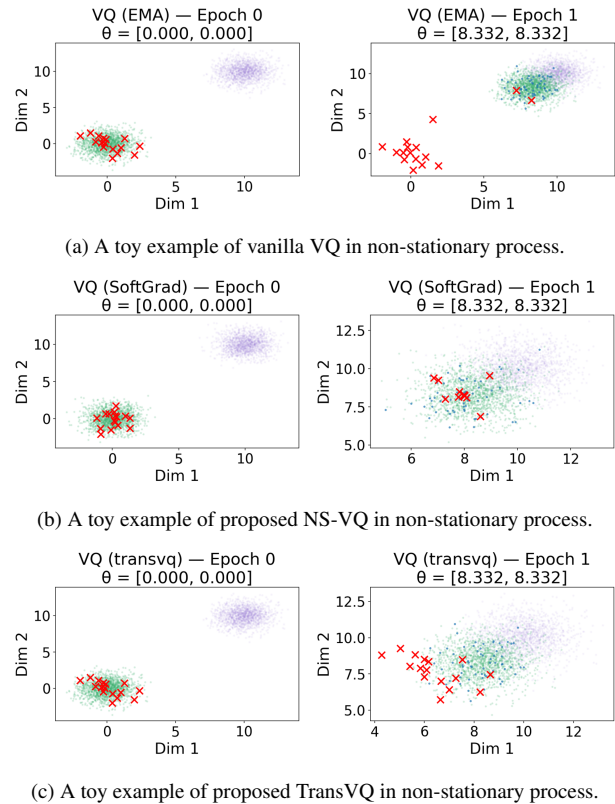


Figure 1. Illustration of codebook adaptation under non-stationary data. (a) In vanilla VQ, codewords fail to track the drifting data distribution, leading to representation collapse. (b) In the proposed NS-VQ, adaptive variance-controlled updates allow the codebook to follow distributional shifts over time, maintaining coverage and stability. (c) In the proposed TransVQ, a few codewords still lag behind the drifting data distribution, but the projector gradients drive all other codewords to move jointly toward the data, improving overall alignment. In the figures, purple dots denote the target distribution Y_t (least visible), green dots represent the base data X , blue dots indicate the current batch X_b , and red crosses mark the codebook vectors C .

*Corresponding author: Hao.Lu@advocatehealth.org

tokenization is widely adopted in visual-language models (VLMs) [5], where images are discretized into code sequences that can be processed by large language models.

Despite these successes, VQ models face a persistent and widely recognized challenge: codebook collapse. As the codebook size increases, a large portion of code vectors remain inactive during training, leading to poor code utilization. This severely limits the effectiveness of VQ in large-scale generative modeling, where scaling the codebook is expected to improve representation power. While numerous practical solutions have been proposed—such as stochastic quantization, codebook reset strategies, distribution regularization, or external feature initialization—most of them are heuristic in nature. They improve utilization rates in practice but lack theoretical justification. Consequently, even when utilization approaches 100%, the final performance across methods varies significantly. This indicates that our current understanding of the codebook collapse problem remains largely empirical and intuition-driven.

In this paper, we take a new theoretical perspective by analyzing the non-stationary nature of VQ-VAE. We show that encoder updates inherently make the latent representation a non-stationary process, which explains why codebook entries may fail to receive updates and eventually collapse, (see Fig. 1). This connection between non-stationarity and codebook collapse provides, for the first time, a theoretical foundation for understanding the phenomenon.

Building on this insight, we propose two new VQ methods designed to address codebook collapse:

- Non-Stationary VQ (NS-VQ), illustrated in Fig. 2a: introduces a kernel-based approximation that propagates encoder drift to non-selected codes, thereby increasing codebook utilization without breaking theoretical convergence conditions.
- Transformer-based VQ (TransVQ), illustrated in Fig. 2b: employs a lightweight mapping function $P_\varphi(\cdot)$ that adaptively transforms the entire codebook in response to encoder updates.

Unlike prior methods such as SimVQ that rely solely on linear mappings and lose convergence guarantees, TransVQ preserves the theoretical conditions for convergence to the k-means solution while ensuring smooth adaptation of all codes.

We evaluate these methods on image reconstruction tasks within the VQ-VAE framework. Experimental results show that both NS-VQ and TransVQ significantly improve reconstruction quality, as measured by rFID, LPIPS, and SSIM, while maintaining nearly complete codebook utilization. Furthermore, our analysis of batch-size effects empirically validates the theoretical predictions of our non-stationary framework.

Our contributions can be summarized as follows:

- We provide a theoretical analysis showing that the non-stationary nature of encoder updates is the root cause of codebook collapse in VQ-VAE.
- We propose NS-VQ, a novel variant that propagates encoder drift to non-selected codes via a kernel-based update rule, ensuring improved utilization.
- We propose TransVQ, which leverages a learnable codebook mapping function that preserves k-means convergence conditions and effectively adapts the entire codebook.
- We conduct extensive experiments on image reconstruction benchmarks, demonstrating that both methods achieve higher utilization and superior reconstruction quality compared to baseline VQ methods.

2. Related Work

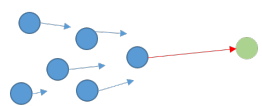
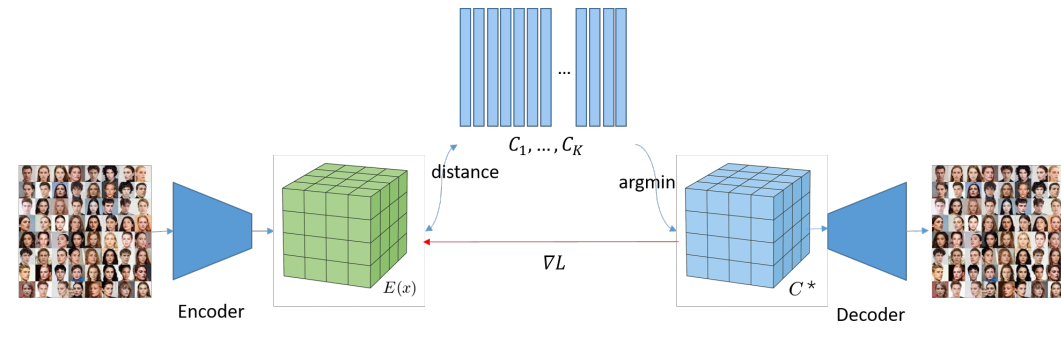
Since its introduction as a stochastic approximation (SA) of k-means [1] and later application to Variational Autoencoders (VQ-VAE) by [2], Vector Quantization (VQ) has become a fundamental building block in modern visual generative models and image tokenization frameworks. It serves as the core component in models such as VQ-GAN [6], LDM [4], and VLM [7], bridging continuous visual features and discrete token representations [8]. Alongside these applications, a rich body of research has explored improving the optimization and utilization of VQ in neural networks.

2.1. Optimization strategies

Several studies have sought to improve the optimization process of VQ models. Huh [9] proposed an alternating optimization scheme that separately updates the encoder and quantization layers to accelerate convergence, albeit with increased computational cost. Baeviski et al. (2019) [10] introduced the Gumbel-Softmax trick, providing a differentiable approximation to the discrete argmin operation during codeword selection. More recently, the rotation trick [11] reformulated the mapping from latent features to codebook vectors as a joint rotation-and-scaling transformation, allowing gradient computation through geometric reparameterization.

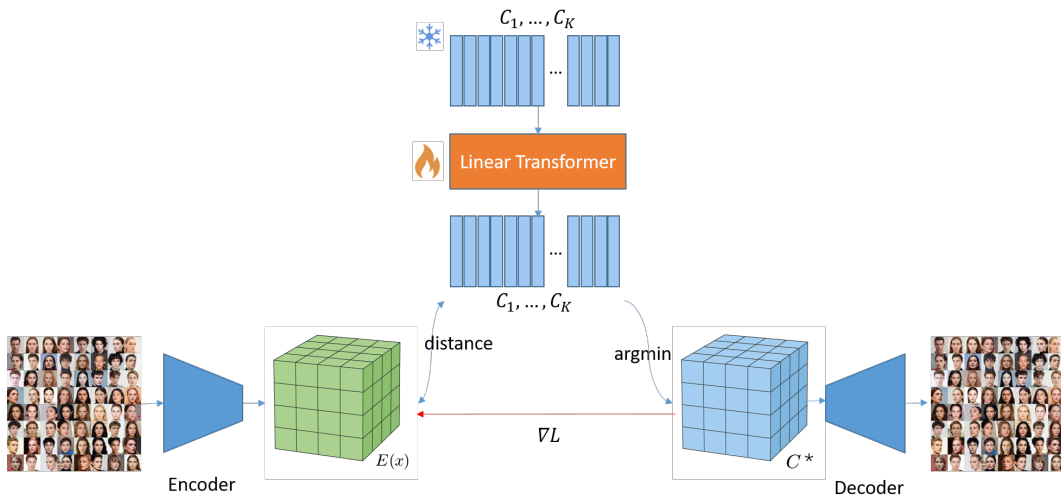
2.2. Improving codebook utilization

Several approaches have been developed to address codebook collapse. Yu [3] proposed maintaining the codebook in a lower-dimensional latent space to increase utilization. SoundStream [12] introduced a dynamic replacement policy that substitutes rarely used codes with randomly sampled vectors from the current batch. SimVQ [13, 14] reparametrized the codebook as a linear transformation CW, enabling gradients to flow to non-winner code vectors and achieving high utilization with a simple design. Other works improve utilization through additional constraints, such as orthogonality regularization [15] and



$$\begin{aligned}
 L'_{emb} &= \|sg(E(x_i)) - c_{q_i}\|^2 \\
 &+ \sum_{q_j \neq q_i} \frac{1}{2} \exp\left(-\frac{\|c_{q_j} - E(x_i)\|^2}{2\sigma^2}\right) \|E(x_i) - c_{q_j}\|^2
 \end{aligned}$$

(a) Scheme of the proposed NS-VQ module, which models non-stationary codebook dynamics through variance-controlled updates.



(b) Scheme of TransVQ, which introduces transformer-based codebook interaction for non-stationary quantization.

Figure 2. Scheme of the proposed (a) Non-Stationary Vector Quantization (NS-VQ) and (b) the Transformer-based Vector Quantization (TransVQ).

cosine-similarity penalties [3]. In contrast, some methods move away from the stochastic k-means formulation entirely—for instance, FSQ [16], which performs scale-based quantization, and LFQ [5], which employs directional (sign-based) clustering.

2.3. Alternative quantization approaches

Beyond codebook optimization, extensions such as residual VQ [12] aim to reduce quantization error by applying multi-stage residual encoding. Our work differs in focus: rather than introducing heuristic improvements, we theoretically analyze the cause of codebook collapse and propose two methods—NS-VQ and TransVQ—that preserve the convergence property of VQ to the k-means solution. SimVQ in-

spires TransVQ, yet we extend it with a theoretical explanation of why codebook mapping mitigates collapse and modify it to maintain k-means convergence. Finally, although our experiments employ the standard straight-through estimator (STE), both proposed methods are fully compatible with the Gumbel-Softmax and rotation-trick frameworks.

3. Method

3.1. Preliminaries

A Vector-Quantized Variational Autoencoder (VQ-VAE) is a reconstructive encoder–decoder architecture that introduces a vector quantization (VQ) layer to convert continuous latent representations into discrete codes. We as-

sume that data $x \in R^d$ is sampled from dataset $X = \{x_1, \dots, x_N\}$, Let set the encoder of the VQ-VAE is denoted to $E_\theta(x) \in \mathbb{R}^d$, and $C = (c_1, \dots, c_K) \in (R^d)^K$ where K is the number of code vectors. We define the Jacobian matrix (linear approximation of encoder changes with respect to parameters) as $J_\theta(x) = \frac{\partial E_\theta(x)}{\partial \theta}$. The Voronoi partition associated with codebook C is $V_k(C) = \{x : \|x - c_k\| \leq \|x - c_j\|, \forall j\}$. For each sample x_i , its assigned code index is denoted by q_i , where $x_i \in V_{q_i}(C)$.

Since the quantization step is non-differentiable, the straight-through estimator (STE) [3] is applied to enable gradient flow. Specifically, the quantized representation is expressed as:

$$Q_e(x_i) = E_\theta(x_i) + \text{sg}(c_{q_i} - E_\theta(x_i))$$

where Q_e is VQ layer output. This yields $(\partial Q_e(x_i))/\partial E(x_i) = 1$.

The overall training objective of VQ-VAE combines reconstruction and commitment losses:

$$L = \log p(x | Q_e) + \|\text{sg}(E_\theta(x)) - c_q\|_2^2 + \beta \|E_\theta(x) - c_q\|_2^2$$

, where the first term is typically the mean squared error (MSE):

$$\log p(x | Q_e) = \|x - g_\psi(Q_e)\|_2^2$$

where $g_\psi(\cdot)$ is the decoder of VAE. Here, the commitment loss encourages the encoder to stay close to the chosen embedding, while the codebook loss ensures that code vectors move toward the encoder outputs.

3.2. Non-stationarity of VQ-VAE and Its Effect on the Quantization Process

We assume k-means initialization, i.e., at iteration $t = 0$, which means initially $C^{(0)}$ fits $c_k^{(0)} = \mathbb{E}[x | x \in V_k(C)]$, where \mathbb{E} means expectation or mean, so that $C^{(0)}$ is k-means solution of the latent space and it is also the locally optimal (a fixed point) of VQ algorithm (proof is in Supplementary 8) if the encoder is frozen.

3.2.1. Non-stationarity in Training

In practice, the encoder parameters θ are updated during training, making $E_{\theta^{(t)}}(x)$ a time-varying, non-stationary random process. This non-stationarity is a key factor in the emergence of “dead” codebook entries in traditional VQ-VAE training. For simplicity, assume batch size = 1 (the reasoning extends naturally to larger batch sizes). When the first sample x_1 is processed, the encoder parameters are updated by backpropagation. Under the straight-through estimator (STE),

$$\Delta\theta^{(0)} = \frac{\partial L}{\partial c_{q_1}^{(0)}} I \frac{\partial E_\theta(x_1)^{(0)}}{\partial \theta^{(0)}} \quad (1)$$

where L is the reconstruction loss. At the same time, the selected codebook entry is updated by the embedding loss:

$$L_{\text{emb}}^{(t)} = \frac{1}{d} \|\text{sg}(E_\theta(x_n)^{(t)}) - c_{q_n}^{(t)}\|^2 \quad (2)$$

leading to

$$c_{q_m}^{(1)} = \begin{cases} c_{q_m}^{(0)} + \eta_0(x_1 - c_{q_m}^{(0)}), & m = 1, \\ c_{q_m}^{(0)}, & m \neq 1 \end{cases} \quad (3)$$

Consider the next sample x_2 , assumed (without loss of generality) to belong to a different Voronoi cell than x_1 . After the encoder update,

$$E_{\theta^{(1)}}(x_2) \approx E_{\theta^{(0)}}(x_2) + J_{\theta^{(0)}}(x_2)\Delta\theta^{(0)} \quad (4)$$

Since $c_{q_2}^{(1)}$ was not updated in the previous step, $c_{q_2}^{(1)} = c_{q_2}^{(0)}$. However, the Jacobian term may cause $E_{\theta^{(1)}}(x_2)$ to fall outside its original Voronoi region $V_{q_2}(C)$. As a result, $c_{q_2}^{(1)}$ may never be selected for updates, eventually becoming a “dead” code.

This mechanism explains the early codebook collapse phenomenon observed in [9] [Fig. 9]. We further illustrate this with toy examples (in supplementary 11 and 7), showing how encoder shifts (translation, scaling, splitting) can cause persistent dead codes. Intuitively, as the encoder parameters evolve, the mapping from inputs to latent space shifts, causing previously used codebook entries to become obsolete.

3.2.2. Effect of Batch Size

From this reasoning, a larger batch size should alleviate codebook collapse: in the first few iterations, more code vectors receive updates, increasing codebook utilization. In the extreme case, if batch size equals dataset size, all code vectors would be updated each iteration, eliminating dead codes entirely. We validated this intuition experimentally by testing VQ-VAE reconstruction performance under different batch sizes (see Fig. 4).

3.3. Method 1: Non-Stationary Vector Quantization (NS-VQ)

We propose Non-Stationary Vector Quantization (NS-VQ) to address the problem of dead codes caused by encoder non-stationarity. NS-VQ modifies the codebook update rule so that unused codes also receive meaningful updates, thereby mitigating early collapse.

3.3.1. Motivation

At t step the encoder is updated with input x_i , the representation of other samples like x_j becomes

$$E_{\theta^{(t)}}(x_j) = E_{\theta^{(t)}}(x_j) + \Delta E_\theta(x_j) \quad (5)$$

where we use a linear approximation to estimate the additional term

$$\Delta E_\theta(x_j) \approx J_{\theta^{(t)}}(x_j)\Delta\theta^{(0)} \quad (6)$$

may cause $E_{\theta^{(t)}}(x_j)$ to fall outside its original Voronoi region, leaving its codebook entry c_{q_j} unused. To counter this, we add a corresponding update to the codebook:

$$\Delta c_{q_j} = \begin{cases} \frac{\partial L_{emb}}{\partial c_{q_j}}, & q_j = q_i, \\ \Delta E(x_j), & q_j \neq q_i. \end{cases} \quad (7)$$

where L_{emb} is the standard embedding loss.

3.3.2. Estimating $\Delta E(x)$

Since only x_i is available in the current batch, we approximate $\Delta E(x_j)$ for other codes q_j using the gradient update from x_i . From one gradient descent step:

$$\Delta\theta = -\eta \frac{\partial L(E_\theta(x_i))}{\partial \theta} = -\eta J_\theta(x_i)^T g_i \quad (8)$$

where $(g_i = \frac{\partial L}{\partial E}(E_\theta(x_i)))$. Then, for any x_j :

$$\Delta E_\theta(x_j) \approx J_\theta(x_j)\Delta\theta \quad (9)$$

$$= -\eta J_\theta(x_j)J_\theta(x_i)^T g_i \quad (10)$$

$$= -\eta K_\theta(x_j, x_i)g_i \quad (11)$$

where $K_\theta(x_j, x_i) = J_\theta(x_j)J_\theta(x_i)^T$ being the neural tangent kernel (NTK). Using $\Delta\theta \approx J_\theta(x_i)^{-1}\Delta E_\theta(x_i)$ to approximate $\Delta\theta$, we can get

$$\Delta E(x_j) \approx K_\theta(x_j, x_i)K_\theta(x_i, x_i)^{-1}\Delta E(x_i) \quad (12)$$

Since computing the NTK is intractable, we approximate it by a Gaussian RBF kernel:

$$k(x_j, x_i) = \exp\left(-\frac{\|E(x_j) - E(x_i)\|^2}{2\sigma^2}\right) \quad (13)$$

Thus,

$$\Delta E(x_j) = \exp\left(-\frac{\|E(x_j) - E(x_i)\|^2}{2\sigma^2}\right)\Delta E(x_i) \quad (14)$$

In practice, we approximate the distance by replacing $E(x_j)$ with its code vector c_{q_j} , and Interestingly, we found that simple substitution $\Delta E(x_i)$ with $(x_i - c_{q_j})$ works better than the full NTK-based estimate.

$$\Delta E(x_j) \approx \exp\left(-\frac{\|E(x_i) - c_{q_j}\|^2}{2\sigma^2}\right)(E(x_i) - c_{q_j}) \quad (15)$$

This leads to a practical and effective update rule:

$$\Delta c_q = \begin{cases} \frac{\partial L_{emb}}{\partial c_{q_j}}, & q_j = q_i, \\ \exp\left(-\frac{\|E(x_i) - c_{q_j}\|^2}{2\sigma^2}\right)(E(x_i) - c_{q_j}), & q_j \neq q_i. \end{cases} \quad (16)$$

This update can be derived from an auxiliary embedding loss:

$$L'_{emb} = \|sg(E(x_i)) - c_{q_i}\|^2 + \sum_{q_j \neq q_i} \exp\left(-\frac{\|E(x_i) - c_{q_j}\|^2}{2\sigma^2}\right)(E(x_i) - c_{q_j}) \quad (17)$$

where $sg(\cdot)$ is the stop-gradient operator.

3.3.3. Modified STE

It is worth noting that we also revisit the update rule in [9] [Eq. (21)], which proposed a ‘‘delay-free’’ correction term for updating $c_{q_i}^{(0)}$ based on $E(x_i)^{(1)} - c_{q_i}^{(0)}$. That method, however, required tuning an additional hyperparameter v , which limits its practical applicability. In our approach, we re-derive a similar correction without the need for extra hyperparameters. The full derivation and proof are provided in the supplementary 9. Shortly, we updated straight-through estimator (STE) for better update c_{q_i} as:

$$Q_e = E(x_i) + sg(c_{q_i} - E(x_i)) + \frac{2}{d}c_{q_i} - sg\left(\frac{2}{d}c_{q_i}\right) \quad (18)$$

where d is the multiplication of batch size and patch numbers at latent feature. In summary, compared with traditional VQ, NS-VQ differs in three aspects:

- New embedding loss introduces cross-updates for non-selected codes.
- Modified STE improves stability under encoder drift.

As shown in Fig. 3, these changes significantly improve reconstruction quality, with further details provided in the next section.

3.4. Method 2: Transformer-based Vector Quantization (TransVQ)

We propose a second approach, called Transformer-based Vector Quantization (TransVQ). The idea is simple: if encoder updates add a drift term to feature representations, why not apply a learnable transformation to the codebook as well?

3.4.1. Motivation

For any sample x_j , the encoder update at iteration t can be written as

$$E_{\theta^{(t+1)}}(x_j) = E_{\theta^{(t)}}(x_j) + J_{\theta^{(t)}}(x_j)\Delta\theta^{(t)} \quad (19)$$

where

$$\Delta E_{\theta^{(t)}}(x_j) = J_{\theta^{(t)}}(x_j)\Delta\theta^{(t)} \quad (20)$$

Instead of leaving the codebook fixed, we introduce a mapping function $P_\phi(\cdot)$ that transforms the codebook:

$$C' = P_\phi(C) \quad (21)$$

During training, only ϕ is updated, while the base codebook C remains unchanged. After an update on a batch x_i , not only is its corresponding transformed code $P_\phi(c_{q_i})$ updated, but all codes are simultaneously updated as

$$P_{\phi^{(t+1)}}(c_{q_j}) = P_{\phi^{(t)}}(c_{q_j}) + J_{\phi^{(t)}}(c_{q_j})\Delta\phi^{(t)} \quad (22)$$

where,

$$J_{\phi^{(t)}}(c_{q_j}) = \frac{\partial P_{\phi^{(t)}}(c_{q_j})}{\partial \phi^{(t)}} \quad (23)$$

3.4.2. Key Observation

In principle, one could explicitly enforce the alignment between encoder and codebook updates by introducing an additional constraint term

$$L_{align} = \|J_{\phi^{(t)}}(c_{q_m})\Delta\phi^{(t)} - J_{\phi^{(t)}}(x_m)\Delta\theta^{(t)}\|^2, \quad (24)$$

but this would dramatically increase computational complexity and is practically infeasible. Interestingly, our experiments reveal that no such explicit constraint is necessary: the standard embedding loss

$$L_{emb} = \|sg(E(x_i)) - c_{q_i}\|^2 \quad (25)$$

alone is sufficient to guide $P_\phi(\cdot)$ so that nearly all codebook entries remain active.

Across all tested variants of $P(\cdot)$, this implicit alignment consistently improves both codebook utilization and reconstruction performance.

3.4.3. Design of $P_\phi(\cdot)$

The mapping $P_\phi(\cdot)$ must be sufficiently generalizable to produce a transformed codebook

$$C' = P_\phi(C) \in \mathbb{R}^d \quad (26)$$

without introducing structural constraints that would break the convergence conditions of VQ to k-means (as proven in Supplementary 8). Notably, this is the key different between TransVQ and methods from [13, 14]. They force $C' = WC$, which adds another condition, making VQ not converge to the k-means solution anymore. A simple example is that we set the dimension of C as 1, then $C' = wC$. Since C is frozen, C' is unlikely to be the k-means solution of $E(x)$. For this reason, we adopt a lightweight transformer block as $P_\phi(\cdot)$:

- Each code vector is treated as a token,
- Passed through a single-head linear attention layer,
- Followed by a small MLP layer.

The output defines the transformed codebook C' .

Table 1. Encoder and decoder architecture of the proposed model.

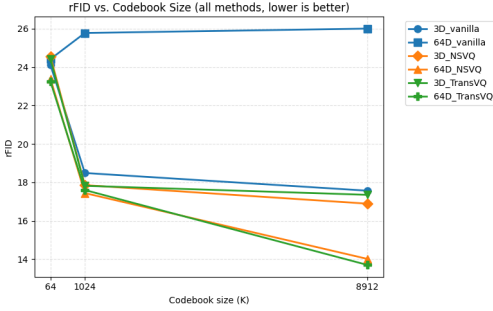
Encoder	Decoder
Conv2d (3→128, k=4, s=2, p=1), LeakyReLU	Conv2d (64→256, k=3, s=1, p=1), LeakyReLU
Conv2d (128→256, k=4, s=2, p=1), LeakyReLU	ResidualLayer ×6 (256→256)
Conv2d (256→256, k=3, s=1, p=1), LeakyReLU	LeakyReLU
ResidualLayer ×6 (256→256)	ConvTranspose2d (256→128, k=4, s=2, p=1), LeakyReLU
LeakyReLU	ConvTranspose2d (128→3, k=4, s=2, p=1), Tanh
Conv2d (256→64, k=1, s=1), LeakyReLU	-

4. Experiments

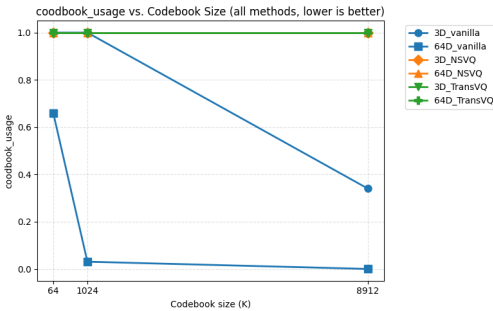
Although our approach can be extended to classification and generative tasks involving VQ, in this work we focus on evaluating NS-VQ and TransVQ within the VQ-VAE framework for image reconstruction. Since our goal is to validate the proposed hypotheses, extensive training under varied hyperparameter settings is required. This makes it impractical to conduct experiments on very large-scale datasets such as ImageNet. Instead, we adopt the CelebA-HQ (256×256) dataset, which contains 30,000 high-quality celebrity face images resampled to 256 pixels. Originally introduced by NVIDIA [17], this dataset is widely used for generative modeling and contains only images without attributes or labels. Additional results on ImageNet are provided in the Supplementary 12 . The encoder and decoder architectures of VQ-VAE follow the design shown in Tab 1. We employ MSE loss as the reconstruction objective, and evaluate reconstruction quality using rFID, LPIPS, and SSIM metrics. We set batch size as 16, learning rate as 0.0005, use Adam optimizer. For NS-VQ, the hyperparameter $2\sigma^2$ was initialized to 1 and decayed by a factor of 0.9 after each epoch. For TransVQ, we used a single linear transformer layer with one attention head, a model dimension of 256, and an MLP ratio of 2. All models were trained for 40 epochs on the training set, and their performance was evaluated on the validation set.

5. Results

From Fig. 3, we observe that NS-VQ and TransVQ do not suffer from the counterintuitive phenomenon seen in VQGAN-FC [3], where reducing the codebook dimension improves reconstruction performance. Instead, our methods increase codebook utilization as predicted by theory, leading to improved reconstruction quality. Tabs. 2 and 3 provides a detailed comparison of rFID across different codebook sizes and embedding dimensions, along with the corresponding codebook utilization. Tab. 4 further com-



(a) rFID vs. Codebook Size (lower is better).



(b) Codebook Usage vs. Codebook Size (higher is better).

Figure 3. Comparison of the proposed NS-VQVAE and TransVQ-VAE with VQGAN-FC [3] under varying codebook sizes. (a) rFID comparison showing both NS-VQVAE and TransVQVAE consistently reduce reconstruction error compared with VQGAN-FC [3]. (b) Codebook utilization indicating that both proposed methods maintain nearly full codebook usage, effectively preventing codebook collapse.

Table 2. Comparison of different VQ methods with 3D code dimension under varying codebook sizes. Results are reported in terms of reconstruction FID (rFID, lower is better) and codebook usage (higher is better).

Method	64		1024		8912	
	rFID	Usage	rFID	Usage	rFID	Usage
VQGAN-FC [3]	24.10	1.00	18.48	1.00	17.57	0.34
VQVAE2 [18]	53.25	1.00	31.17	0.40	24.24	0.60
VQGAN-EMA [19]	60.86	1.00	17.86	1.00	17.93	1.00
SimVQ [19]	23.39	1.00	23.35	1.00	21.69	1.00
NS-VQ	24.55	1.00	17.86	1.00	16.89	1.00
TransVQ	24.42	1.00	17.82	1.00	17.35	1.00

compares rFID, LPIPS, and SSIM for different VQ methods under their optimal codebook configurations. Finally, Fig. 4 shows the rFID curves of the standard VQ-VAE, with the codebook size and dimension fixed at 64, under varying batch sizes. The consistent decrease in rFID with larger batch sizes empirically supports our theoretical analysis.

Table 3. Comparison of different VQ methods with 64D code dimension under varying codebook sizes. Results are reported in terms of reconstruction FID (rFID, lower is better) and codebook usage (higher is better).

Method	64		1024		8912	
	rFID	Usage	rFID	Usage	rFID	Usage
VQGAN-FC [3]	24.41	0.66	25.77	0.03	26.00	0.00
VQVAE2 [18]	85.86	0.82	36.91	0.57	25.87	0.28
VQGAN-EMA [19]	159.21	1.00	20.81	1.00	19.39	1.00
SimVQ [13]	23.40	1.00	17.77	1.00	14.37	1.00
NS-VQ	23.39	1.00	17.44	1.00	14.01	1.00
TransVQ	23.24	1.00	17.60	1.00	13.70	1.00

Table 4. Detailed comparison of VQ methods at their best-performing configurations (as determined by rFID in Table 2 and Table 3). Results are reported in terms of SSIM (higher is better), LPIPS (lower is better), and rFID (lower is better).

Method	Codebook Size	Code Dim	SSIM	LPIPS	rFID
VQGAN-FC [3]	8912	3	0.93	0.022	17.57
VQVAE2 [18] (3D)	8912	3	0.89	0.042	24.24
VQGAN-EMA [19]	1024	3	0.92	0.024	17.86
SimVQ [13]	8912	64	0.93	0.017	14.37
NS-VQ	8912	64	0.96	0.015	14.01
TransVQ	8912	64	0.94	0.015	13.70

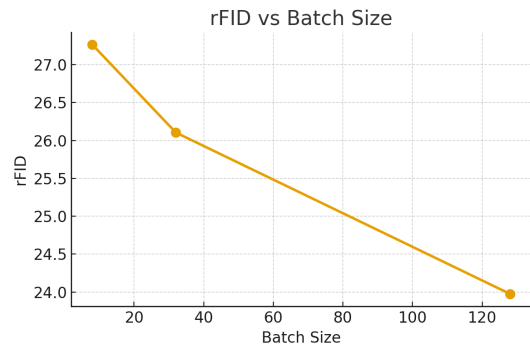


Figure 4. rFID curves of standard VQ-VAE with codebook size and code dimension fixed at 64, evaluated under different batch sizes. Larger batch sizes lead to lower rFID values, consistent with our theoretical analysis that larger batches provide more stable codebook updates.

6. Discussion

In this work, we restrict our comparison to VQ methods that converge to the k-means solution. Many recent variants have deviated from the stochastic approximation of k-means; for example, FSQ [16] performs direct quantization of latent features rather than clustering, while Lfq [7] can be regarded as sign or directional clustering. These methods are therefore excluded from our evaluation. In Eq. 17, we

proposed replacing $\Delta E(x_i)$ with $(x_i - c_{q_j})$. In the Supplementary 10 provides a derivation for directly using $\Delta E(x_i)$, which also improves traditional VQ in practice and may be of interest for further exploration.

We also note certain limitations. NS-VQ, while theoretically grounded, requires tuning the hyperparameter $2\sigma^2$, which typically must decay with training iterations—making the optimization process more complex. In contrast, TransVQ is easier to tune but introduces additional computational cost. Interestingly, we observed that replacing the transformer block with a two-layer MLP slightly reduces performance but significantly improves speed, which may be useful in practice.

Finally, we would like to point out an open question regarding the common practice of VQ initialization and training. Most existing works—including ours—first initialize the codebook using k-means and then perform online updates through the VQ layer until convergence to the k-means solution in the latent space. However, this raises a natural question: if a global k-means step is already performed, why not simply train a conventional autoencoder, freeze the encoder after training, and then apply k-means on the latent features to obtain the codebook? This approach would even reduce the overall computational cost. One possible explanation is that the quantization layer in VQ-VAE inherently prevents the autoencoder from degenerating into an identity mapping, a problem often encountered in standard AEs. Nevertheless, to the best of our knowledge, there has been no theoretical or empirical study that explicitly analyzes this effect. Understanding why the VQ layer improves representation learning over post-hoc k-means clustering represents an important future direction for VQ-VAE research.

7. Conclusion

In this work, we revisited vector quantization from a theoretical perspective and identified the non-stationary nature of VQ-VAE as the fundamental cause of codebook collapse. Building on this insight, we proposed two new approaches, NS-VQ and TransVQ, that propagate encoder drift to non-selected codes or adapt the entire codebook through a learnable mapping. Both methods preserve the convergence conditions of VQ while significantly improving codebook utilization and reconstruction quality.

Extensive experiments on CelebA-HQ and additional validations demonstrate that NS-VQ and TransVQ consistently outperform standard VQ variants in terms of rFID, LPIPS, and SSIM, while maintaining near-complete codebook usage. Beyond improving empirical performance, our analysis provides a stronger theoretical foundation for understanding and addressing codebook collapse.

Looking forward, the proposed methods can generalize beyond image reconstruction to a wide range of generative

and multimodal tasks where VQ serves as the discrete interface, including large-scale visual-language models. Our work thus bridges the gap between theory and practice in vector quantization, offering new directions for building more scalable and reliable VQ-based models.

Although our methods enhance stability and utilization, they introduce additional hyperparameters (e.g., $2\sigma^2$ and transformer depth) that require careful tuning. Future work could focus on developing adaptive or self-regularizing mechanisms to automatically control these parameters during training. Moreover, integrating NS-VQ and TransVQ into diffusion, autoregressive, and multimodal architectures may further reveal their potential for large-scale generative modeling. Another promising direction is to explore dynamic or hierarchical codebook expansion, allowing the model to flexibly adjust its representational capacity as training progresses. Lastly, a deeper theoretical study of how quantization interacts with gradient flow and representation learning could provide a unified framework for next-generation VQ-based models.

References

- [1] R. Gray, “Vector quantization,” *IEEE Assp Magazine*, vol. 1, no. 2, pp. 4–29, 1984. 1, 2
- [2] A. Van Den Oord and O. Vinyals, “Neural discrete representation learning,” *Advances in neural information processing systems*, vol. 30, 2017. 1, 2
- [3] J. Yu, X. Li, J. Y. Koh, H. Zhang, R. Pang, J. Qin, A. Ku, Y. Xu, J. Baldridge, and Y. Wu, “Vector-quantized image modeling with improved vqgan,” *arXiv preprint arXiv:2110.04627*, 2021. 1, 2, 3, 4, 6, 7
- [4] R. Rombach, A. Blattmann, D. Lorenz, P. Esser, and B. Ommer, “High-resolution image synthesis with latent diffusion models,” in *Proceedings of the IEEE/CVF conference on computer vision and pattern recognition*, 2022, pp. 10 684–10 695. 1, 2
- [5] L. Yu, Y. Cheng, K. Sohn, J. Lezama, H. Zhang, H. Chang, A. G. Hauptmann, M.-H. Yang, Y. Hao, I. Essa *et al.*, “Magvit: Masked generative video transformer,” in *Proceedings of the IEEE/CVF Conference on Computer Vision and Pattern Recognition*, 2023, pp. 10 459–10 469. 2, 3
- [6] P. Esser, R. Rombach, and B. Ommer, “Taming transformers for high-resolution image synthesis,” in *Proceedings of the IEEE/CVF conference on computer vision and pattern recognition*, 2021, pp. 12 873–12 883. 2, 4
- [7] L. Yu, J. Lezama, N. B. Gundavarapu, L. Versari, K. Sohn, D. Minnen, Y. Cheng, V. Birodkar, A. Gupta, and X. Gu, “Language model beats diffusion—tokenizer is key to visual generation,” *arXiv preprint arXiv:2310.05737*, 2023. 2, 7
- [8] M. Caron, P. Bojanowski, A. Joulin, and M. Douze, “Deep clustering for unsupervised learning of visual features,” in *Proceedings of the European conference on computer vision (ECCV)*, 2018, pp. 132–149. 2
- [9] M. Huh, B. Cheung, P. Agrawal, and P. Isola, “Straightening out the straight-through estimator: Overcoming opti-

- mization challenges in vector quantized networks,” in *International Conference on Machine Learning*. PMLR, 2023, pp. 14 096–14 113. [2](#), [4](#), [5](#)
- [10] A. Baevski, S. Schneider, and M. Auli, “vq-wav2vec: Self-supervised learning of discrete speech representations,” *arXiv preprint arXiv:1910.05453*, 2019. [2](#)
- [11] C. Fifty, R. G. Junkins, D. Duan, A. Iyengar, J. W. Liu, E. Amid, S. Thrun, and C. Ré, “Restructuring vector quantization with the rotation trick,” *arXiv preprint arXiv:2410.06424*, 2024. [2](#)
- [12] N. Zeghidour, A. Luebs, A. Omran, J. Skoglund, and M. Tagliasacchi, “Soundstream: An end-to-end neural audio codec,” *IEEE/ACM Transactions on Audio, Speech, and Language Processing*, vol. 30, pp. 495–507, 2021. [2](#), [3](#)
- [13] Y. Zhu, B. Li, Y. Xin, Z. Xia, and L. Xu, “Addressing representation collapse in vector quantized models with one linear layer,” *arXiv preprint arXiv:2411.02038*, 2024. [2](#), [6](#), [7](#), [4](#)
- [14] L. Zhu, F. Wei, Y. Lu, and D. Chen, “Scaling the codebook size of vq-gan to 100,000 with a utilization rate of 99.2,” [2](#), [6](#)
- [15] W. Shin, G. Lee, J. Lee, E. Lyou, J. Lee, and E. Choi, “Exploration into translation-equivariant image quantization,” in *ICASSP 2023-2023 IEEE International Conference on Acoustics, Speech and Signal Processing (ICASSP)*. IEEE, 2023, pp. 1–5. [2](#)
- [16] F. Mentzer, D. Minnen, E. Agustsson, and M. Tschannen, “Finite scalar quantization: Vq-vae made simple,” *arXiv preprint arXiv:2309.15505*, 2023. [3](#), [7](#)
- [17] T. Karras, T. Aila, S. Laine, and J. Lehtinen, “Progressive growing of gans for improved quality, stability, and variation,” *arXiv preprint arXiv:1710.10196*, 2017. [6](#)
- [18] A. Razavi, A. van den Oord, and O. Vinyals, “Generating diverse high-fidelity images with vq-vae-2,” in *Advances in Neural Information Processing Systems*, 2019. [7](#), [4](#)
- [19] P. Esser, R. Rombach, and B. Ommer, “Taming transformers for high-resolution image synthesis,” in *IEEE/CVF Conference on Computer Vision and Pattern Recognition (CVPR)*, 2021. [7](#)
- [20] H. J. Kushner and G. G. Yin, *Stochastic approximation and recursive algorithms and applications*. Springer, 2003. [1](#)
- [21] L. Eon Bottou, “Online learning and stochastic approximations,” *Online learning in neural networks*, vol. 17, no. 9, p. 142, 1998. [1](#)

Beyond Stationarity: Rethinking Codebook Collapse in Vector Quantization

Supplementary Material

8. Proof that VQ Converges to the k -Means Solution

Without loss of generality, assume data $x \in \mathbb{R}^d$ is sampled i.i.d. from a distribution P . The same argument applies to the finite empirical case, replacing integrals by finite sums. We maintain K centroids (or codes) $C = (c_1, \dots, c_K) \in (\mathbb{R}^d)^K$. Given C , define the Voronoi partition:

$$V_k(C) = \{x : \|x - c_k\| \leq \|x - c_j\|, \forall j\}.$$

The expected distortion (quantization error) is

$$\begin{aligned} J(C) &= \mathbb{E}_{x \sim P} \left[\min_k \|x - c_k\|^2 \right] \\ &= \sum_{k=1}^K \int_{V_k(C)} \|x - c_k\|^2 dP(x). \end{aligned} \quad (\text{A1})$$

The k -means problem (and equivalently, VQ codebook design) seeks to minimize $J(C)$. Away from measure-zero tie boundaries, the partition does not change under small centroid moves, so we can differentiate J at regular points:

$$\begin{aligned} \frac{\partial J}{\partial c_k}(C) &= \frac{\partial}{\partial c_k} \sum_{k=1}^K \int_{V_k(C)} \|x - c_k\|^2 dP(x) \\ &= -2 \int_{V_k(C)} (x - c_k) dP(x). \end{aligned} \quad (\text{A2})$$

Setting the gradient to zero gives

$$\begin{aligned} \int_{V_k(C)} x dP(x) &= c_k \int_{V_k(C)} dP(x), \\ \iff c_k &= \mathbb{E}[x \mid x \in V_k(C)]. \end{aligned} \quad (\text{A3})$$

Thus, the stationary points of k -means are those C^* for which every centroid equals the conditional mean of its Voronoi cell—the usual M-step in k -means.

Stochastic Online Update. Consider the standard “winner-take-all” online VQ update for a sample $x_t \sim P$:

$$k_t(x_t) = \arg \min_j \|x_t - c_j^{(t)}\|, \quad (\text{A4})$$

$$c_k^{(t+1)} = c_k^{(t)} + \eta_t \mathbf{1}\{k = k_t(x_t)\}(x_t - c_k^{(t)}), \quad (\text{A5})$$

where η_t is the step size. Taking conditional expectation given $C^{(t)}$:

$$\mathbb{E}[c_k^{(t+1)} - c_k^{(t)} \mid C^{(t)}] = \eta_t h_k(C^{(t)}), \quad (\text{A6})$$

where

$$\begin{aligned} h_k(C) &\triangleq \mathbb{E}[\mathbf{1}\{x \in V_k(C)\}(x - c_k)] \\ &= \int_{V_k(C)} (x - c_k) dP(x). \end{aligned} \quad (\text{A7})$$

Comparing Eq. (A7) with Eq. (A2), we have

$$\frac{\partial J}{\partial c_k}(C) = -2h_k(C).$$

Hence, the mean update direction equals $-\frac{1}{2}\nabla J(C)$, meaning online VQ is a stochastic approximation (SA) to gradient descent of the k -means objective.

We can rewrite the recursion in SA form:

$$c_k^{(t+1)} = c_k^{(t)} + \eta_t (h_k(C^{(t)}) + \xi_{t,k}), \quad (\text{A8})$$

with a martingale-difference noise term

$$\begin{aligned} \xi_{t,k} &= \mathbf{1}\{x_t \in V_k(C^{(t)})\}(x_t - c_k^{(t)}) \\ &\quad - h_k(C^{(t)}), \quad \mathbb{E}[\xi_{t,k} \mid C^{(t)}] = 0. \end{aligned} \quad (\text{A9})$$

Convergence Conditions. The following assumptions hold:

- **Step sizes (Robbins–Monro):** $\sum_t \eta_t = \infty$, $\sum_t \eta_t^2 < \infty$.
- **Boundedness:** Data have bounded second moment and centroids are projected to a compact set.
- **Regularity:** $h(C)$ is locally Lipschitz away from tie boundaries, which form a measure-zero set.

Under these conditions, by standard SA/ODE theory [20, 21], the discrete iterates track the flow of the ODE

$$\dot{C}(t) = h(C(t)) = -\frac{1}{2}\nabla J(C(t)). \quad (\text{A10})$$

Using J as a Lyapunov function:

$$\begin{aligned} \frac{d}{dt} J(C(t)) &= \langle \nabla J(C(t)), \dot{C}(t) \rangle \\ &= -\frac{1}{2} \|\nabla J(C(t))\|^2 \leq 0. \end{aligned} \quad (\text{A11})$$

Therefore, trajectories converge to the stationary set $\{\nabla J = 0\}$. From Eq. (A2), any limit point C^* satisfies

$$c_k^* = \mathbb{E}[x \mid x \in V_k(C^*)], \quad \forall k,$$

which is a k -means fixed point (typically a local minimum). Hence, online VQ with Robbins–Monro step sizes converges almost surely to a k -means solution (local optimum).

9. Modified Straight-Through Estimator (STE)

In the main text, we revisited the update rule proposed in [9] [Eq. (21)], which introduced a ‘‘delay-free’’ correction term for updating $c_{q_i}^{(0)}$ based on $E(x_i)^{(1)} - c_{q_i}^{(0)}$. That method, however, required tuning an additional hyperparameter v , which limits its practical applicability. Here, we derive a similar correction from first principles without introducing new hyperparameters.

9.1. Revisiting the Embedding Loss

In VQ-VAE, the embedding loss at iteration t is

$$L_{\text{emb}}^{(t)}(x_n, c_{q_n}) = \frac{1}{d} \left\| \text{sg}(E(x_n)^{(t)}) - c_{q_n}^{(t)} \right\|^2, \quad (\text{A16})$$

which encourages $c_{q_n}^{(t)}$ to move toward $E(x_n)^{(t)}$. After one iteration, the encoder updates according to

$$E(x_n)^{(t+1)} = E(x_n)^{(t)} + \lambda \frac{\partial L}{\partial E(x_n)^{(t)}}. \quad (\text{A17})$$

The natural question arises: why not directly update $c_{q_n}^{(t)}$ so that it also moves toward the newly updated encoder output $E(x_n)^{(t+1)}$.

9.2. Delay-Free Correction Term

In that case, we define

$$L_{\text{emb}}^{(t)'}(x_n, c_{q_n}) = \frac{1}{d} \left\| \text{sg}(E(x_n)^{(t+1)}) - c_{q_n}^{(t)} \right\|^2. \quad (\text{A18})$$

The gradient with respect to $c_{q_n}^{(t)}$ becomes

$$\begin{aligned} \frac{\partial L_{\text{emb}}^{(t)'}}{\partial c_{q_n}^{(t)}} &= \frac{2}{d} \left(E(x_n)^{(t+1)} - c_{q_n}^{(t)} \right) \\ &= \frac{2}{d} \left(E(x_n)^{(t)} - c_{q_n}^{(t)} \right) + \frac{2\lambda}{d} \frac{\partial L}{\partial E(x_n)^{(t)}}. \end{aligned} \quad (\text{A19})$$

The first term can be obtained directly from the standard embedding loss $L_{\text{emb}}^{(t)}$, while the second term can be propagated to the codebook through the straight-through estimator (STE).

9.3. Modified Quantizer with STE Injection

Using the STE formulation, the quantized output is

$$Q_e = E(x_n)^{(t)} + \text{sg}(c_{q_n}^{(t)} - E(x_n)^{(t)}). \quad (\text{A20})$$

To inject the additional gradient flow from $E(x_n)^{(t)}$ into $c_{q_n}^{(t)}$, we modify the quantizer as

$$\begin{aligned} Q_e &= E(x_n)^{(t)} + \text{sg}(c_{q_n}^{(t)} - E(x_n)^{(t)}) \\ &\quad + \frac{2}{d} c_{q_n}^{(t)} - \text{sg}\left(\frac{2}{d} c_{q_n}^{(t)}\right). \end{aligned} \quad (\text{A21})$$

Here, Q_e denotes the quantization output of the VQ layer. This modification ensures that the gradient of $E(x_n)^{(t)}$ automatically propagates into $c_{q_n}^{(t)}$, achieving a delay-free correction without introducing any new hyperparameters.

10. Alternative Update Using $\Delta E(x)$

In the main text, we proposed a practical approximation that replaces $\Delta E(x_i)$ with $(x_i - c_{q_i})$. Here, we provide the complementary formulation that directly propagates $\Delta E(x)$ to the codebook updates.

10.1. Recap of the Approximation

From the NTK-based derivation, we have

$$\Delta E(x) \approx \exp\left(-\frac{\|x - x_i\|^2}{2\sigma^2}\right) \Delta E(x_i). \quad (\text{A12})$$

Since the future sample x is unavailable at the current iteration, we approximate the distance using code vectors:

$$\|x - x_i\|^2 \approx \|c_q - x_i\|^2. \quad (\text{A13})$$

This approximation allows all codebook entries to be updated in parallel without waiting for additional samples.

10.2. STE-Based Injection

Interestingly, we can inject $\Delta E(x_i)$ into the straight-through estimator (STE) via the stop-gradient trick. Specifically, the quantized embedding can be expressed as

$$\begin{aligned} Q_e &= E(x_i) + \text{sg}(c_{q_i} - E(x_i)) \\ &\quad + \sum_{q_n \neq q_i} (w_n c_{q_n} - \text{sg}(w_n c_{q_n})), \end{aligned} \quad (\text{A14})$$

where the weights are defined as

$$w_n = \exp\left(-\frac{\|c_{q_n} - x_i\|^2}{2\sigma^2}\right). \quad (\text{A15})$$

This formulation distributes a fraction of $\Delta E(x_i)$ across all non-selected codes, thereby alleviating the dead-code problem by ensuring that each code receives gradient information proportional to its similarity to the current sample.

11. Toy Demos for Non-Stationary Vector Quantization

This appendix provides three toy experiments that illustrate how non-stationarity affects vector quantization and how our proposed NS-VQ stabilizes training under dynamic data distributions.

11.1. Toy Demo 1 | Translation Motion

Purpose. Compare two codebook-update rules for vector quantization on a simple non-stationary 2D dataset where a global drift variable θ evolves during training:

- EMA (vanilla VQ update method)
- NS-VQ (our proposed method)

Data and Non-Stationarity.

$$X_{\text{init}} \sim \mathcal{N}(0, I_2), \quad N = 1500, \quad \text{noise scale} = 1.0, \\ \theta \in \mathbb{R}^2, \quad \theta_0 = [0, 0].$$

For each mini-batch with indices idxs :

$$X_b = X[\text{idxs}] + \theta, \quad Y_t^{(b)} = X_{\text{init}}[\text{idxs}] + (10, 10).$$

The drift variable is updated by

$$\theta \leftarrow \theta + r \cdot \text{mean}(Y_t^{(b)} - X_b), \quad r = 0.1.$$

Codebook and Assignment.

$$C \in \mathbb{R}^{16 \times 2}, \quad C \sim \mathcal{N}(0, 1), \quad w_i = \arg \min_k \|x - c_k\|_2^2.$$

Update Rules. (1) EMA Update. If cluster k has assigned samples in the current batch:

$$\bar{y}_k = \frac{1}{|\{i : w_i = k\}|} \sum_{i:w_i=k} X_b^{(i)}, \\ C_k \leftarrow (1 - \alpha)C_k + \alpha \bar{y}_k, \quad \alpha = 0.3.$$

(2) NS-VQ Online Update. Processed sample-by-sample within each mini-batch using temperature τ and learning rate lr:

$$d_k = \|C_k - C_w\|^2, \quad \omega_k = \frac{e^{-d_k/\tau}}{\sum_j e^{-d_j/\tau}}, \\ C_w \leftarrow C_w + \text{lr}(x - C_w), \\ C_k \leftarrow C_k + \text{lr} \omega_k (x - C_k), \quad k \neq w.$$

After each epoch:

$$\tau \leftarrow \frac{1}{2}\tau, \quad \text{lr} \leftarrow 0.9 \text{lr}.$$

11.2. Toy Demo 2 | Expansion / Scaling

Purpose. Compare two codebook-update rules on a non-stationary 2D dataset where the data undergo a global linear scaling learned online via a matrix A .

Data and Target Mapping (Fixed).

$$X_{\text{init}} \sim \mathcal{N}(0, I_2), \quad N = 1500.$$

Draw $M \in \mathbb{R}^{2 \times 2}$ such that $\|M\|_2 > 1$ and define the fixed targets:

$$Y_t = X_{\text{init}} M^T.$$

Learned State and Batch Variables. Initialize $A = I$. For a mini-batch with indices idxs :

$$X_b = X[\text{idxs}], \quad Y_b = Y_t[\text{idxs}], \\ AX_b = X_b A^T, \quad E = Y_b - AX_b.$$

Update of A (exact code):

$$g_A = \frac{2}{B} E^T X_b, \quad (\text{descent direction of } -\nabla_A \|Y_b - AX_b\|_F^2) \\ A \leftarrow A + r g_A, \quad r = 0.1.$$

All other settings are identical to Appendix 11.1. We also tested a *shrink* variant by setting $\|M\|_2 < 1$.

11.3. Toy Demo 3 | Split (Quadrant Separation)

Purpose. Compare the two update rules on a 2D dataset where samples split by sign into opposite quadrants and drift scales by coordinate sign.

Data, Target, and Non-Stationarity.

$$X_{\text{init}} \sim \mathcal{N}(\mu, \sigma^2 I_2), \quad \mu = [0.5, 0.5], \quad \sigma = 1.0, \\ Y_t = X_{\text{init}} + 10 \cdot \text{sign}(X_{\text{init}}).$$

Initialize drift $\theta = [0, 0]$. For each batch:

$$X_b = X[\text{idxs}], \\ X_b \leftarrow X_b + \text{sign}(X_b) \odot \theta, \\ \theta \leftarrow \theta + r \cdot \text{mean}(Y_t^{(b)} - X_b), \quad r = 0.1.$$

For visualization, the full cloud at each step is

$$X_b + \text{sign}(X_b) \odot \theta.$$

12. Results on ImageNet

We employ a Taming-style convolutional encoder–decoder architecture without self-attention, consisting of three resolution stages. The VQ-VAE model is trained on ImageNet-1K at a resolution of 256×256 using a batch size of 12 and Adam optimizers with $\beta_1 = 0.5$ and $\beta_2 = 0.9$. The base learning rate is set to 4.5×10^{-6} . The reconstruction objective combines mean squared error (MSE) and LPIPS loss. All hyperparameter settings for NS-VQ and TransVQ follow those described in Section 4. Each experiment is trained for four epochs.

13. Qualitative Reconstructions

Figure 5 presents side-by-side reconstructions for six methods: ground-truth (GT), vanilla VQ-VAE, EMA-VQ, NS-VQ (ours), SimVQ, and TransVQ (ours). Consistent with the quantitative results in the main paper, both NS-VQ and TransVQ recover finer facial detail and textures while

Table 5. VQ-VAE architecture (Taming-style, attention-free). The encoder and decoder are symmetric with residual connections.

Encoder	Decoder
Conv2d (3→128, k=4, s=2, p=1), LeakyReLU	Conv2d (3→512, k=3, s=1, p=1), LeakyReLU
ResidualBlock ×2 (128→128)	ResidualBlock ×2 (512→512)
Conv2d (128→256, k=4, s=2, p=1), LeakyReLU	ConvTranspose2d (512→256, k=4, s=2, p=1), LeakyReLU
ResidualBlock ×2 (256→256)	ResidualBlock ×2 (256→256)
Conv2d (256→512, k=4, s=2, p=1), LeakyReLU	ConvTranspose2d (256→128, k=4, s=2, p=1), LeakyReLU
ResidualBlock ×2 (512→512)	ResidualBlock ×2 (128→128)
Conv2d (512→3, k=3, s=1, p=1) → quant.conv (1×1, 3→embed_dim=3)	post_quant_conv (1×1, embed_dim=3→3)
—	Conv2d (128→3, k=3, s=1, p=1), Tanh

Table 6. Quantitative comparison on ImageNet-1K at 256 × 256 resolution. Lower rFID and LPIPS indicate better reconstruction quality and perceptual fidelity.

Method	rFID	LPIPS
VQGAN [6]	1.060	0.113
VQGAN-FC [3]	0.600	0.087
VQGAN-EMA [18]	1.270	0.124
SimVQ [13]	0.551	0.088
NS-VQ (ours)	0.561	0.087
TransVQ (ours)	0.432	0.067

avoiding over-smoothing. In particular, NS-VQ reduces blocky artifacts by maintaining active code utilization, and TransVQ preserves high-frequency cues (hair strands, eye contours) via its codebook transform.



(a) Ground truth (GT).



(b) Vanilla VQ-VAE.



(c) EMA-VQ.



(d) NS-VQ (ours).



(e) SimVQ.



(f) TransVQ (ours).

Figure 5. **Qualitative reconstruction comparison.** Each strip shows the same set of identities. NS-VQ and TransVQ maintain sharp edges and facial micro-structure while reducing artifacts observed in vanilla and EMA-VQ. This aligns with the quantitative gains in rFID/LPIPS/SSIM reported in the main paper.

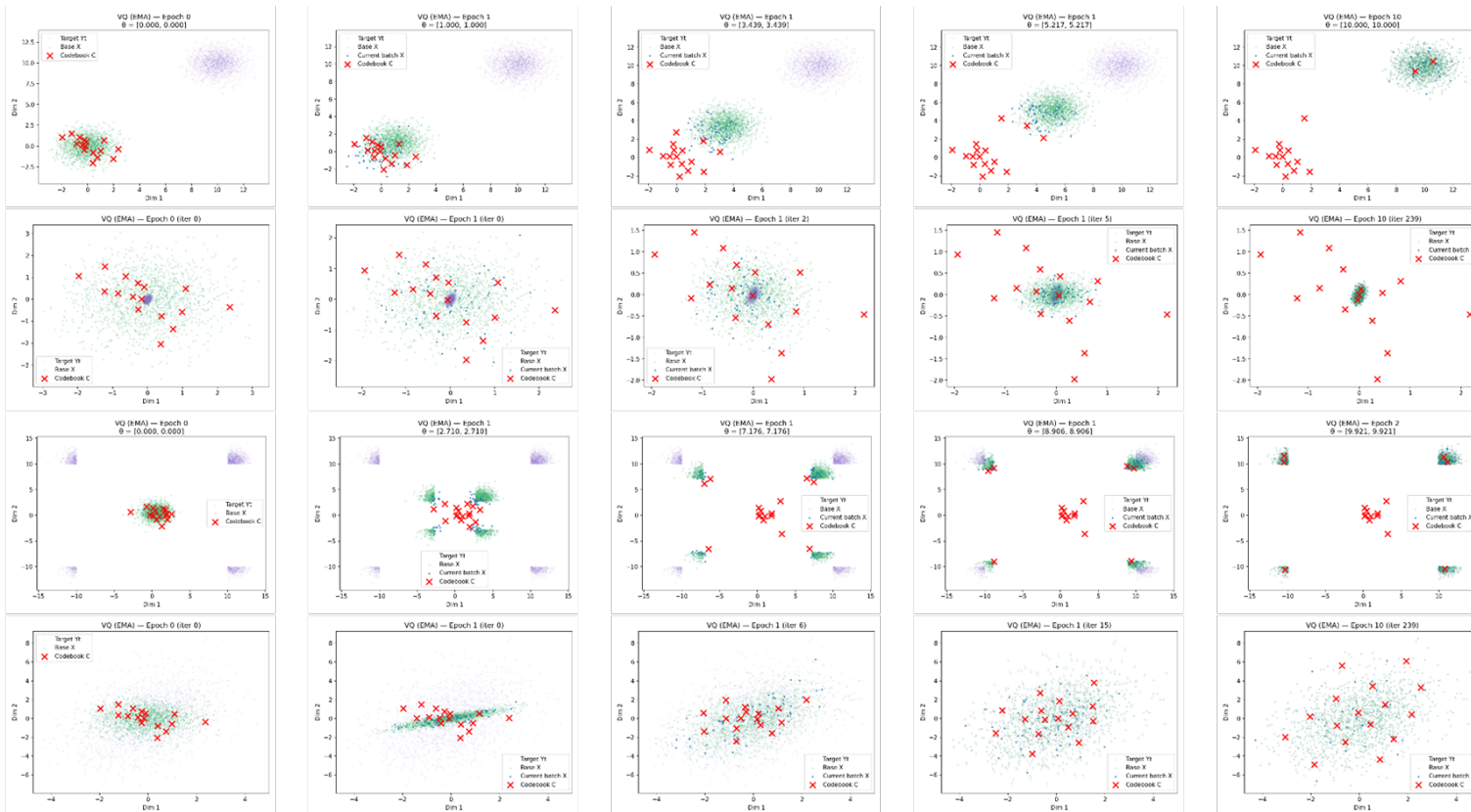


Figure 6. **Toy Demo Visualization for Vanilla VQ.** Each row corresponds to one toy experiment: translation (1st row), shrink (2nd row), split (3rd row), and expansion (4th row). Each row contains five snapshots showing the convergence process across training steps.

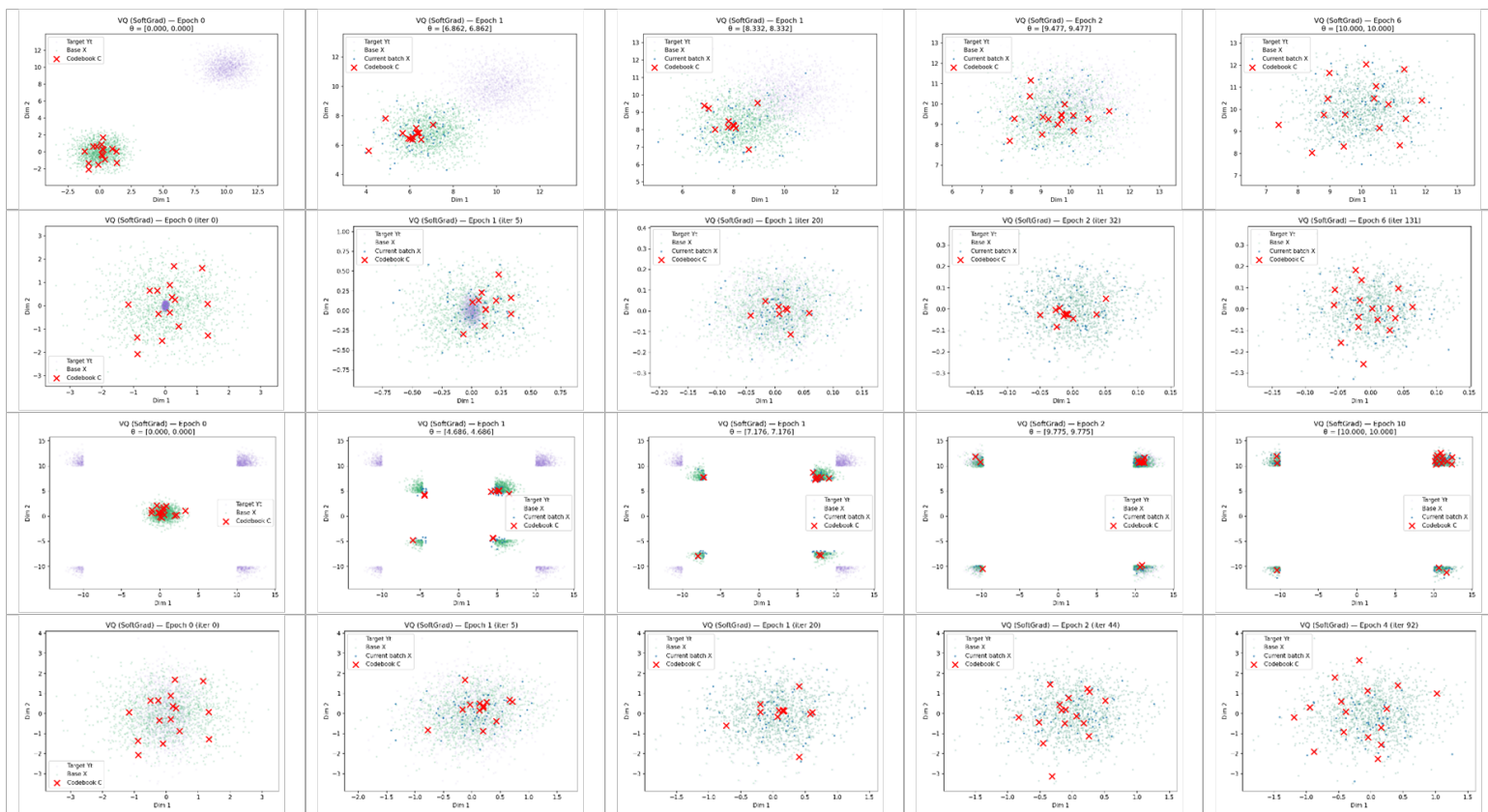


Figure 7. **Toy Demo Visualization for NS-VQ.** Each row corresponds to one toy experiment: translation (1st row), shrink (2nd row), split (3rd row), and expansion (4th row). Each row contains five snapshots showing how NS-VQ maintains stability and codebook utilization during convergence.